

New Journal of Physics

The open access journal at the forefront of physics

Deutsche Physikalische Gesellschaft  IOP Institute of Physics

Published in partnership
with: Deutsche Physikalische
Gesellschaft and the Institute
of Physics



PAPER

OPEN ACCESS

RECEIVED
18 January 2018

REVISED
22 March 2018

ACCEPTED FOR PUBLICATION
6 April 2018

PUBLISHED
11 May 2018

Phase transition kinetics for a Bose Einstein condensate in a periodically driven band system

E Michon¹, C Cabrera-Gutiérrez¹, A Fortun¹, M Berger¹, M Arnal¹, V Brunaud¹, J Billy¹, C Petitjean², P Schlagheck² and D Guéry-Odelin¹

¹ Université de Toulouse; UPS; Laboratoire Collisions Agrégats Réactivité, IRSAMC; F-31062 Toulouse, France

² Département de Physique, CESAM research unit, University of Liege, B-4000 Liège, Belgium

E-mail: dgo@irsamc.ups-tlse.fr

Keywords: quantum gas, optical lattice, phase transition

Original content from this work may be used under the terms of the [Creative Commons Attribution 3.0 licence](#).

Any further distribution of this work must maintain attribution to the author(s) and the title of the work, journal citation and DOI.



Abstract

The dynamical transition of an atomic Bose–Einstein condensate from a spatially periodic state to a staggered state with alternating sign in its wavefunction is experimentally studied using a one-dimensional phase modulated optical lattice. We observe the crossover from quantum to thermal fluctuations as the triggering mechanism for the nucleation of staggered states. In good quantitative agreement with numerical simulations based on the truncated Wigner method, we experimentally investigate how the nucleation time varies with the renormalized tunneling rate, the atomic density, and the driving frequency. The effective inverted energy band in the driven lattice is identified as the key ingredient which explains the emergence of gap solitons as observed in numerics and the possibility to nucleate staggered states from interband excitations as reported experimentally.

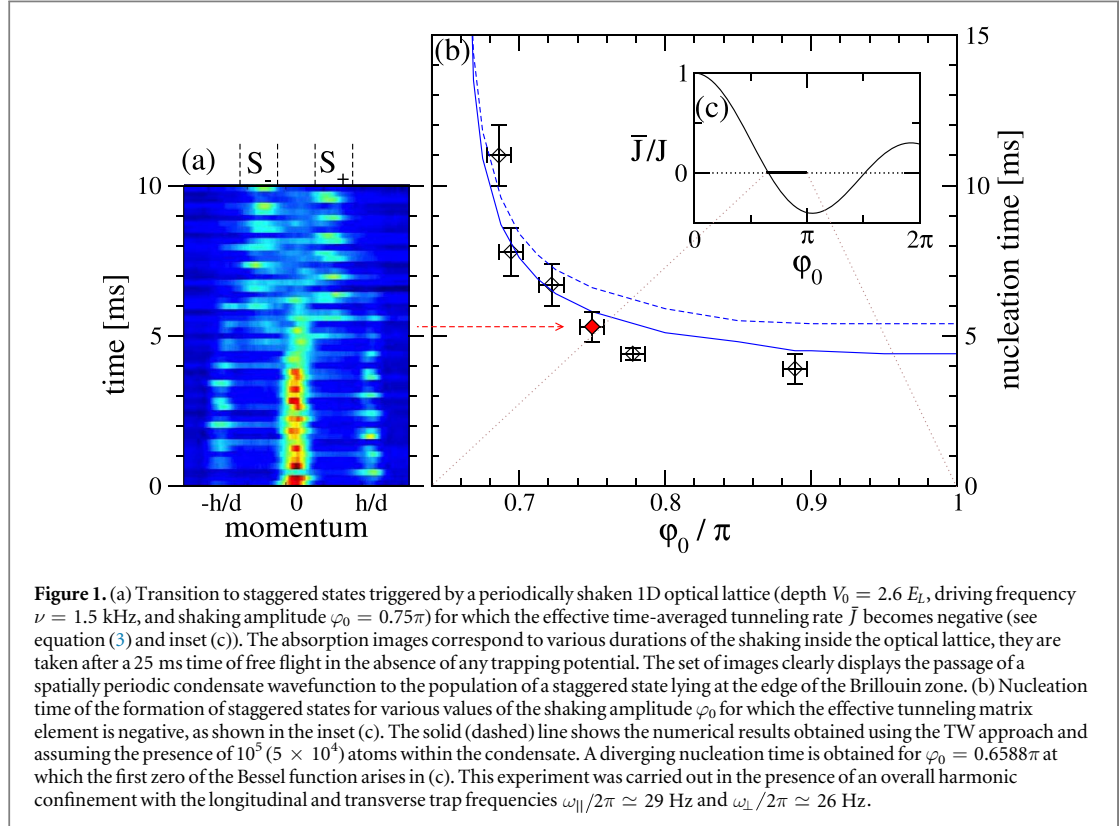
1. Introduction

Cold atoms in optical lattices provide powerful and versatile platforms for quantum simulators of many-body systems [1–4], and give access to the rich out-of-equilibrium dynamics of such systems. A remarkable progress for tunability was achieved by exposing lattice potentials to a time-periodic driving, whereby an effective renormalization of the tunneling rate between adjacent sites can be induced [5–7]. This opened many new perspectives for quantum simulations with the possibility to engineer effective Hamiltonians and study topological phases [8]. Recent examples include the realization of the Hofstadter [9] and Haldane models [10] as well as the investigation of frustrated magnetism [11].

While the single-particle physics appears to be well explored in this context, present-day state-of-the-art experiments focus on the investigation of many-body effects in driven lattices [12, 14, 15]. Indeed, interactions between the atoms in the gas are of particular interest as they may trigger dynamical quantum phase transitions in the presence of the driving, e.g., to a ferro- or antiferromagnetic state of the gas [12, 15]. This opens new avenues for engineering topological properties of many-body states. However, enhancing the role of interactions within a cold Bose gas can also give rise to a loss of spatial and many-body coherence [13, 14]³, which poses additional challenges for the controllability of the resulting state.

To explore the interplay of such interaction-induced transitions with the potential loss of coherence properties in an elementary context, we focus on a Bose–Einstein condensate (BEC) that is prepared in a one-dimensional (1D) optical lattice. A periodic shaking of the lattice is switched on with an amplitude for which the renormalized tunneling matrix element becomes negative. The quantum gas is thereby put in a metastable situation inside the 1D optical lattice. The presence of interactions will then trigger a dynamical instability which changes the nodal structure of the underlying wavefunction by inducing a transition from a periodic state (without nodes) to an antiperiodic or *staggered* state (with regularly spaced nodes) for which neighboring sites acquire opposite phases [5, 6, 17–19]. This phase transition can be readily observed in momentum space after a

³ The term *many-body coherence* refers here to Glauber’s notion of coherence [16] applied to the Fock space of identical bosonic atoms. For instance, a BEC can be represented by a perfectly coherent state, while a thermal or Fock state is incoherent in this sense.



time of flight expansion [20], where it manifests itself in form of new interference peaks at the edge of the Brillouin zone that arise in between the ordinary static peaks (see figure 1(a)), as observed for instance in [5, 6, 11]. Interestingly, despite its spatial interferability the resulting staggered state does no longer exhibit many-body coherence (see footnote 4), which implies that this transition is not quantitatively accounted for with a standard mean-field approach.

In this article, we experimentally investigate the nucleation of such states in a 1D shaken optical lattice and compare our result with Bogoliubov and truncated Wigner (TW) calculations. Our experiments are complementary to nucleation studies of vortices in a rotating BEC [21–23], which provides another example of phase transition triggered by a dynamical instability [24, 25]. In those latter experiments, however, the kinetics of the transition could not be studied as a function of the density since the rotation weakens the transverse 2D confinement. We report hereafter a variation by one order of magnitude of the nucleation time of staggered states with the atomic density, and investigate experimentally and numerically the role of the renormalized tunneling rate and the modulation frequency on the out-of-equilibrium dynamics. We clearly identify the triggering mechanism through quantum or thermal fluctuations. We finally determine the range of frequency over which this nucleation can be observed and report on an accelerated transition to staggered states near interband resonances within the lattice.

2. Dynamical instability in a driven Bose–Hubbard system

Our experiments were realized on our rubidium-87 BEC machine that relies on a hybrid (magnetic and optical) trap [26]. The pure BEC of 10^5 atoms in the $F = 1, m_F = -1$ state is loaded in a horizontal 1D optical lattice (lattice spacing $d = 532$ nm) by superposing two counterpropagating lasers. The lattice modulation of the intensity occurs along the x axis referred to as the longitudinal axis in the following. The relative phase between the two lasers is modulated so that the atoms experience the potential

$$V(x, y, z, t) = \frac{1}{2}m(\omega_{||}^2x^2 + \omega_{\perp}^2(y^2 + z^2)) - \frac{V_0}{2}\left[1 + \cos\left(\frac{2\pi x}{d} + 2\varphi_0 \sin(2\pi\nu t)\right)\right], \quad (1)$$

where $\omega_{||}$ (resp. ω_{\perp}) accounts for the longitudinal (resp. transverse) confinement of the hybrid trap and m is the mass of the atoms.

To obtain a first theoretical understanding, we perform a gauge transformation to the comoving frame in which the lattice is periodically tilted instead of shaken. This gauge transformation can be explicitly expressed in terms of the unitary operator

$$T(t) = \exp\left(\frac{2i}{\hbar}vmd\varphi_0 \cos(2\pi\nu t)x\right) \exp\left(-\frac{d}{\pi}\varphi_0 \sin(2\pi\nu t)\frac{\partial}{\partial x}\right) \quad (2)$$

to be applied to the bosonic field operator of the many-body system. The single-particle Hamiltonian describing an atom in the above time-periodic potential is then transformed according to $H(t) \mapsto T(t)H(t)T^{-1}(t) + i\hbar\dot{T}(t)T^{-1}(t)$. In this new representation, we limit ourselves to the single-band approximation, which is valid for $V_0 < 4\pi\varphi_0 mv^2 d^2$. The motion of the atoms along the lattice is first modeled by a 1D tight-binding Hamiltonian in which each well of the lattice is represented by one site. This Hamiltonian is constituted by site-dependent on-site energies given by the longitudinal confinement of the trap, as well as by an approximately site-independent inter-site hopping matrix element J that depends on the strength of the lattice.

As a result of the modulation, this inter-well tunneling rate J is renormalized by a Bessel function

$$\bar{J} = J \times J_0(2\pi\varphi_0 h\nu/E_L), \quad (3)$$

where $E_L = h^2/(2md^2)$ is the lattice characteristic energy⁴. This result is readily derived from a one-body analysis [27–29] but turns out to remain valid in the presence of two-body interactions [19]. A qualitative picture of the impact of this renormalization can be worked out perturbatively with the expression for the energy of the lowest band using the Peierls substitution: $E_0(k) = -2\bar{J} \cos(kd)$. For $\bar{J} > 0$ the minimum of the band is located at $k = 0$, and the Fourier transform of the wave function consists in a comb of peaks centered about $k = 0$ with a spacing $2\pi/d$. For $\bar{J} < 0$, the minima are located on the border of the Brillouin zone at $k = \pm\pi/d$.

When the sign of \bar{J} is suddenly changed through phase modulation, the system is therefore put in a metastable state. While this would not affect the mean-field dynamics of a BEC in the presence of a translationally invariant lattice, any deviation from perfect homogeneity in the condensate wavefunction or the lattice will give rise to a shrinking amplitude of the periodic condensate mode and to an exponentially increasing population of staggered modes at $k = \pm\pi/d$. This mechanism, through which two atoms starting with zero momentum acquire finite momenta of opposite sign, is an example of spontaneous four-wave mixing [5, 6, 17–19]. This elementary process occurs similarly in a condensate of 10^5 atoms where it can apply to any pair of atoms.

A qualitative understanding of this dynamical instability can be obtained from the homogeneous Bose–Hubbard Hamiltonian

$$\hat{H} = -\bar{J} \sum_{l=-\infty}^{\infty} (\hat{b}_l^\dagger \hat{b}_{l+1} + \hat{b}_{l+1}^\dagger \hat{b}_l) + \frac{U}{2} \sum_{l=-\infty}^{\infty} \hat{b}_l^\dagger \hat{b}_l^\dagger \hat{b}_l \hat{b}_l, \quad (4)$$

where \hat{b}_l denotes the annihilation operator associated with the Wannier function centered on the l th well of the lattice and U accounts for a site-independent two-body interaction strength. Assuming the presence of a perfectly homogeneous condensate at $t = 0$ exhibiting n atoms per site, we make the Bogoliubov ansatz

$$\hat{b}_l(t) = \left[\sqrt{n} + \sqrt{\frac{d}{2\pi}} \int_{-\pi/d}^{\pi/d} \hat{\Lambda}(k, t) e^{ikd} dk \right] e^{-i\mu t/\hbar}, \quad (5)$$

where $\mu = -2\bar{J} + nU$ is the chemical potential of the condensate. Following [30], we hereby introduce the (number-conserving) de-excitation operator $\hat{\Lambda}(k, t)$ which transfers an atom from an excited state with finite quasimomentum $kd \neq 0$ back to the condensate characterized by $k = 0$, while its adjoint operator $\hat{\Lambda}^\dagger(k, t)$ would revert this process. Linearizing the resulting equation for $\hat{\Lambda}(k, t)$ yields

$$i\hbar \frac{\partial}{\partial t} \hat{\Lambda}(k, t) = 2\bar{J}(1 - \cos kd) \hat{\Lambda}(k, t) + nU[\hat{\Lambda}(k, t) + \hat{\Lambda}^\dagger(-k, t)] \quad (6)$$

whose solution evolves sinusoidally in time according to

$$\begin{aligned} \hat{\Lambda}(k, t) = & \left[\cos\Omega_k t - \frac{2i\bar{J}}{\Omega_k} (1 - \cos kd) \sin\Omega_k t \right] \hat{\Lambda}(k, 0) \\ & - \frac{inU}{\Omega_k} [\hat{\Lambda}(k, 0) + \hat{\Lambda}^\dagger(-k, 0)] \sin\Omega_k t \end{aligned} \quad (7)$$

⁴The characteristic energy is given by $E_L = 4E_{\text{rec}}$ where $E_{\text{rec}} = h^2/(2m\lambda^2)$ is the recoil energy associated with the absorption of one photon with wavelength $\lambda = 2d$ from one of the laser beams that generate the lattice.

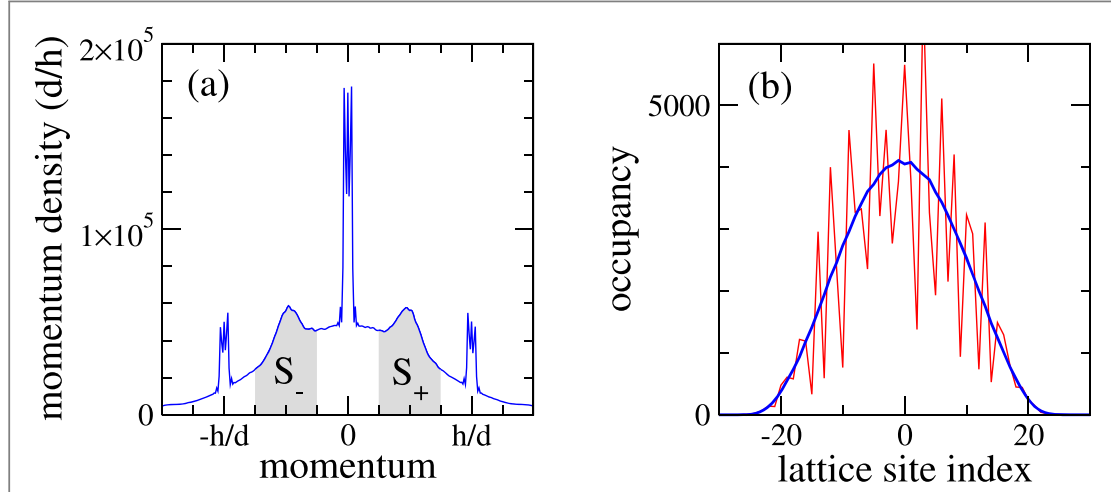


Figure 2. Numerically computed mean momentum density (a) and mean numbers of atoms on the lattice sites (b, blue line) at the evolution time $t = 7.5$ ms in the presence of a shaking with the frequency $\nu = 1.5$ kHz and the amplitude $\varphi_0 = 0.75\pi$, calculated with the TW method for a BEC containing 10^5 atoms (lattice depth $V_0 = 2.6E_L$). The shaded areas in (a) correspond to the staggered mode populations S_+ and S_- . The light gray (red) line in panel (b) shows the occupancies that are obtained by computing a single TW trajectory. It indicates that the population of staggered states is accompanied by strong fluctuations of the lattice site occupancies.

with the Bogoliubov phonon frequencies

$$\Omega_k = \frac{1}{\hbar} \sqrt{4\bar{J}(1 - \cos kd)[\bar{J}(1 - \cos kd) + nU]}. \quad (8)$$

The time-dependent population of non-condensed modes can then be directly evaluated in the Heisenberg representation using the commutator $[\hat{\Lambda}(k, 0), \hat{\Lambda}^\dagger(k', 0)] = \delta(k - k')$ as well as the fact that excited modes with $k \neq 0$ are unpopulated in the initial state. This straightforwardly yields

$$\langle \hat{\Lambda}^\dagger(k, t)\hat{\Lambda}(k', t) \rangle = (nU)^2 \left(\frac{\sin \Omega_k t}{\Omega_k} \right)^2 \delta(k - k'). \quad (9)$$

A dynamical instability occurs when \bar{J} becomes negative. In that case, Ω_k becomes imaginary for each quasiparticle mode that satisfies the relation $\bar{J}(1 - \cos kd) < 0 < \bar{J}(1 - \cos kd) + nU$, which according to equation (9) implies that tiny initial populations of such modes experience an exponential growth with time. For $nU > -4\bar{J}$, this growth is most pronounced for the staggered Bogoliubov modes defined by $kd = \pm\pi$, which describe an antiperiodic Bloch function within the lattice; the population of these staggered modes grows with the Lyapunov exponent $\lambda = [-8\bar{J}(2\bar{J} + nU)]^{1/2}/\hbar$.

In practice, the dominant deviations from translational invariance required to trigger the instability are provided by quantum or thermal fluctuations⁵. This can be verified by numerical simulations of the time evolution of the condensate using the TW method [31]. This method, implemented here within the single-band approximation at zero temperature, accounts for the effect of quantum fluctuations about the initial coherent state of the condensate, and is adapted to take into account the inhomogeneities of the confinement and the finite size of the BEC (see appendix A). Applied to the Bose–Hubbard Hamiltonian (4), it essentially amounts to sampling the time evolution of the quantum bosonic many-body state in terms of classical trajectories that evolve according to a discrete Gross–Pitaevskii equation.

The transition to staggered states is quantitatively characterized by the *nucleation time* representing the instance at which the population of a periodic condensate state within the shaken lattice becomes less significant than the population of a staggered state with antiperiodic nature. To this end, we define by P_0 the population of the central condensate peak located at $k = 0$, and by S_\pm the staggered states population about $\pm h/(2d)$ in momentum space. In the numerical simulations, P_0 and S_\pm are determined by integrating the momentum-space density $\rho(k) = n(k)a_{||}\exp(-k^2a_{||}^2)/(\pi^{1/2}d)$ within the intervals $-\pi/2d < k < \pi/2d$ and $-\pi/2d < k \mp \pi/d < \pi/2d$, respectively, where $n(k)$ is the $2\pi/d$ -periodic momentum density that results from the TW simulation of the Bose–Hubbard dynamics (see shaded areas in figure 2(a)). The nucleation time is defined by

⁵ We should note that a qualitatively similar transition from a periodic to a staggered state can also arise on the level of the mean-field dynamics of the condensate described by the Gross–Pitaevskii equation, namely if the spatial homogeneity of the lattice is perturbed by the presence of an additional confinement. For the experimental parameters at hand, however, this perfectly coherent effect is entirely overshadowed by the depletion of the condensate arising due to the presence of quantum or thermal fluctuations.

the time beyond which $S_+ + S_-$ exceeds P_0 . It corresponds to the instance at which the peaks at $k = \pm\pi/d$ have the same accumulated contrast as the peak at $k = 0$ in the experimental absorption images.

3. Experimental findings and comparison with numerical simulations

The first experimental study that we performed deals with the nucleation time of staggered states for different values of the renormalized tunneling rate \bar{J} in the regime where it acquires negative values. As predicted by the expression for the Lyapunov exponent, we indeed observed a strong increase of the nucleation time when we approach an amplitude of modulation that corresponds to the zero of the Bessel function (see figure 1(c)). Good agreement is obtained with TW computations of the nucleation time indicated by the solid (dashed) lines in figure 1(b), which were conducted according to the above prescriptions assuming the presence of 10^5 (5×10^4) atoms in the condensate⁶. As these simulations were performed at zero temperature, thermal fluctuations seem to play a minor role in this set of data. This is indeed consistent with time-of-flight measurements that we carried out for this parameter regime, which could only yield an upper value estimation $T < 5\text{nK}$ for the temperature.

The evolution of the atomic gas in momentum space is illustrated in figure 1(a) which shows a sequence of time-of-flight absorption images taken after various evolution times. We clearly see the transition from an initially coherent BEC, characterized by a sharp central peak at $k = 0$ and by two side peaks at $k = \pm 2\pi/d$, to a cloud that oscillates between two maxima at $k = \pm\pi/d$. These latter peaks are significantly broader than the initial condensate peaks, which is indicative of an effective increase of the temperature as a consequence of the dynamical instability mechanism [14, 19, 32, 33]. As shown in figure 2(a), this is also observed in the TW simulations, which also reveal that many-body coherence is lost in those side peaks (see appendix A). The sharp coherent BEC peaks at $k = 0$ and $\pm 2\pi/d$ are still present in the numerical simulations, in contrast to the experiment where they are nearly completely washed out after the nucleation. We attribute this to the single-band approximation that we apply in our TW approach and to the effect of quantum fluctuations in the transverse degrees of freedom within the lattice [34], which are not accounted for in the numerical simulations.

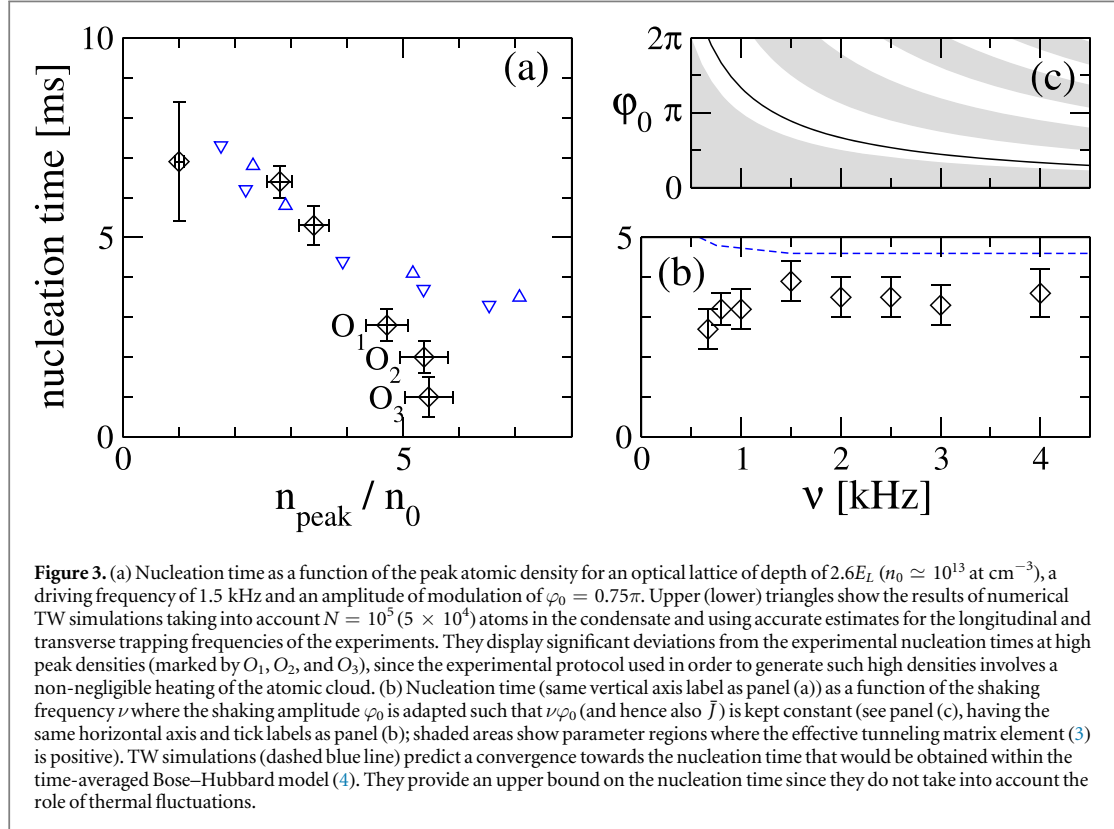
The TW approach allows one to obtain complementary insight into the nature of the staggered states that would not be easily accessible in the experiment. This concerns, in particular, the behavior of lattice site occupancies. While their mean values $\langle \hat{n}_l \rangle = \langle \hat{b}_l^\dagger \hat{b}_l \rangle$ do not display any notable feature in the course of the time evolution, their rms widths $(\langle \hat{n}_l^2 \rangle - \langle \hat{n}_l \rangle^2)^{1/2}$ dramatically increase as soon as staggered states become significantly populated. This is illustrated in figure 2(b) where the mean lattice site occupancies (averaged over 10 000 trajectories) are plotted together with the occupancies that were obtained from a single trajectory (shown in red), at an evolution time $t = 7.5\text{ ms}$ that exceeds the nucleation process. We see pronounced spatial fluctuations of the lattice site occupancies. They give rise to an enhancement of the interaction energy contained within the atomic gas, which compensates for the loss of kinetic energy that is entailed by the transition to staggered states in the presence of the driving.

The occurrence of such spatial fluctuations is strongly reminiscent of *gap solitons* [35] and indicates that the formation of staggered states in momentum space is accompanied by the generation of solitons. This interpretation is consistent with the Bogoliubov mode analysis in a 1D shaken optical lattice of [19]. It is further confirmed by the fact that the spatial extension of the density peaks is indeed on the order of the theoretical prediction $\sigma \simeq 2.6d[2|\bar{J}|/(n_{\max} U)]^{1/2} \simeq 0.7d$ for the full width at half maximum (FWHM) of a gap soliton according to [35] with $n_{\max} \simeq 5000$ the maximal occupancy within a lattice site (see appendix B for a more detailed account on such gap solitons). In our specific (three-dimensional) experimental context, these gap solitons are expected to quickly disintegrate into vortices and vortex rings through the snake instability [36]. By preparing the condensate in highly elongated (cigar-shaped) trapping potentials, they can be stabilized. However, their observation would require an *in situ* imaging with an optical resolution on the order of 500 nm.

To explore the dependence of the nucleation time on the atomic density, we performed experiments where we changed the intensity of the vertical beam of the crossed dipole trap after the BEC production. In this manner, we could vary the atomic peak density between 5.5×10^{13} at cm^{-3} and 10^{13} at cm^{-3} and⁷ observe a large variation of the nucleation time. As shown in figure 3(a), the experimental results are in good agreement with TW simulations, except for high peak densities $n_{\text{peak}} \gtrsim 5 \times 10^{13}$ at cm^{-3} . Indeed, to induce such high densities we compress adiabatically the trap and therefore increase the temperature. From the data point O_1 to the data point O_2 in figure 3(a) the temperature is doubled, and it is further enhanced by a factor 1.6 from O_2 to the data point O_3 yielding $T_{O_3} \simeq 13\text{ nK}$. Thanks to this protocol, we clearly observe the onset of the role of thermal fluctuations in the nucleation process. This is to be contrasted with the low density regime where the nucleation is consistently explained by quantum fluctuations solely. Such a quantitative comparison of

⁶ We estimate to have between 5×10^4 and 10^5 atoms in our experimentally prepared Bose–Einstein condensates.

⁷ The calibration of the density was confirmed by an *in situ* on-resonance strong intensity absorption imaging as described in [37].

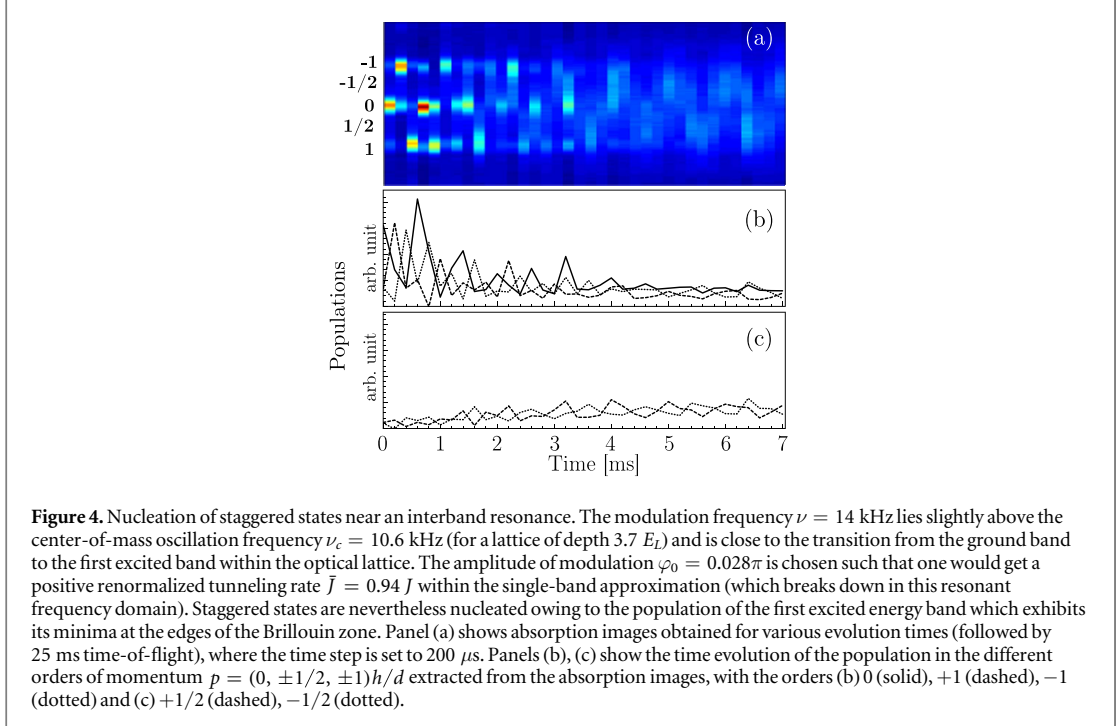


experimental data with a theoretical approach at zero temperature without adjustable parameters remains the only method to identify the crossover between quantum and thermal fluctuations.

Finally, we investigate in figure 3(b) the dependence of the nucleation time with the driving frequency ν where we adapt the shaking amplitude $\varphi_0 = (0.889\pi/\nu) \times 1.5$ kHz such that the argument of the Bessel function is kept constant according to equation (3) yielding $\bar{J} \simeq -0.33J$. As we have the same time-averaged Bose–Hubbard Hamiltonian (4) for all ν , the nucleation time is found to vary only rather weakly with the driving frequency. This behavior is expected to change for $\nu \sim \nu_c$ where ν_c corresponds to the center of mass oscillation frequency (see appendix C) [26]. Spanning the interval $0 < \nu < \nu_c$, we could nucleate staggered states only for a frequency ν below $\sim\nu_c/2$ (see figure 3(b) with $V_0 = 2.6E_L$ and $\nu_c = 8.1$ kHz, and appendix D), which defines experimentally the range of validity of the single band approximation. However, changing the driving parameters such that $\bar{J} > 0$ can give rise to a resurgence of nucleation near the interband resonance. For a lattice depth $V_0 = 3.7E_L$, a modulation frequency $\nu = 14$ kHz and $\varphi_0 = 0.028\pi$ a fast transition to staggered states within 2.7 ms was observed, as shown in figure 4. We attribute this to the population of the first excited band triggered by quantum or thermal fluctuations, which for $\bar{J} > 0$ has an inverted parabolic shape near $k = 0$ and exhibits its minima at $k = \pm\pi/d$ in the Brillouin zone. The numerical study of the appearance of staggered states in this frequency regime therefore requires a more involved treatment taking into account higher bands.

4. Conclusion

In summary, we presented an experimental study of the dynamical transition of a BEC from periodic to staggered states within a periodically shaken optical lattice. As was revealed by TW simulations, this transition is accompanied by a global loss of many-body coherence, even though spatial interferability between different lattice sites is still preserved. It is triggered by quantum or thermal fluctuations, depending on the temperature within the BEC. As key ingredient we identified the inversion of the effective energy band in momentum space, which exhibits a maximum in the center and minima at the edges of the Brillouin zone. This inversion is responsible for the formation of density fluctuations within the lattice that are closely related to gap solitons. The presence of an inverted energy-momentum dispersion relation lies also at the heart of the rapid nucleation of staggered states observed for positive renormalized tunneling near interband resonances, which involve the population of the first excited band within the lattice.



The present experimental setting can be exploited in order to yield a quantitative diagnostic tool for determining interaction and fluctuation effects in similar dynamical transitions involving, e.g. ferro- or antiferromagnetic states [15]. Further studies in the high-frequency regime will be interesting in order to explore the nucleation of staggered states through near-resonant interband transitions in more detail.

Acknowledgments

We thank J Dalibard, N Goldman, H Lignier and M Oberthaler for useful discussions. This work was supported by Direction Générale de l'Armement (DGA), Programme Investissements d'Avenir ANR-11-IDEX-0002-02, reference ANR-10-LABX-0037-NEXT, and by the Programme Hubert Curien 2016.

Appendix A. Implementation of the TW method

The starting point for the implementation of the TW method is the effective many-body Bose–Hubbard Hamiltonian

$$\hat{H}(t) = -J \sum_{l=-\infty}^{\infty} [\hat{b}_l^\dagger \hat{b}_{l+1} e^{-i\theta(t)} + \hat{b}_{l+1}^\dagger \hat{b}_l e^{i\theta(t)}] + \sum_{l=-\infty}^{\infty} \left[V_l \hat{b}_l^\dagger \hat{b}_l + \frac{U_l}{2} \hat{b}_l^\dagger \hat{b}_l^\dagger \hat{b}_l \hat{b}_l \right] \quad (\text{A.1})$$

which describes the dynamics of a BEC within a periodically shaken lattice. Here we employ a single-band approximation within the reference frame that is comoving with the shaken lattice. The shaking is incorporated by means of a periodically time-dependent Peierls phase

$$\theta(t) = 2\pi\varphi_0 \frac{\hbar\nu}{E_L} \cos(2\pi\nu t) \quad (\text{A.2})$$

within the inter-site hopping matrix elements of the lattice. The on-site energies

$$V_l = \frac{1}{2} m \omega_{||}^2 d^2 l^2 \quad (\text{A.3})$$

account for the presence of the longitudinal harmonic confinement with the oscillation frequency $\omega_{||}$.

For lattice strengths $V_0 = s E_L$ with $s \gtrsim 2$, we can approximately represent the Wannier function within the l th well by the Gaussian

$$\Phi_l(x) = \frac{1}{\sqrt{\pi^{1/2} a_0}} \exp \left[-\frac{(x - ld)^2}{2a_0^2} \right], \quad (\text{A.4})$$

where

$$a_0 = \sqrt{\frac{\hbar}{m\omega_0}} = \frac{\sqrt{2s^{-1/2}}}{k} \quad (\text{A.5})$$

is the oscillator length associated with the frequency $\omega_0 = s^{1/2}E_L/\hbar$ of oscillations within each well of the lattice. The effective hopping parameter between adjacent wells can be determined from a semiclassical Wentzel–Kramers–Brillouin (WKB) ansatz [38, 39]. We obtain

$$J = \frac{\hbar\omega_0}{\sqrt{e\pi}} e^{-\sigma} \quad (\text{A.6})$$

with the dimensionless imaginary action

$$\begin{aligned} \sigma &= \sqrt{2s} \int_{\arccos\eta}^{\pi} \sqrt{\eta - \cos u} \, du \\ &= \sqrt{8s(\eta + 1)} E \left[\frac{\pi - \arccos\eta}{2}, \sqrt{\frac{2}{\eta + 1}} \right], \end{aligned} \quad (\text{A.7})$$

where we introduce the parameter

$$\eta = \exp \left(-\frac{1}{2s^{1/2}} \right) - \frac{1}{2s^{1/2}} \quad (\text{A.8})$$

and the incomplete elliptic integral of the second kind $E(\varphi, k) = \int_0^\varphi \sqrt{1 - k^2 \sin^2 \theta} \, d\theta$. Note that this WKB ansatz is based on the approximate expression $E_0 = (1 - \eta)s^{1/2}\hbar\omega_0/2$ for the ground state energy within each well, which is obtained from the expression (A.4) for the Wannier function using first-order perturbation theory.

A complication is introduced by the fact that the lattice wells in the experiment are not truly 1D but rather exhibit a pancake shape, as the transverse confinement frequency ω_\perp of the trap is comparable to the longitudinal one ω_\parallel and hence much larger than ω_0 . For the total atom numbers at hand, the BEC exhibits a parabolic Thomas–Fermi profile in its transverse density distribution within lattice wells that are located near the center of the trap. The interaction energy within such a well therefore scales in a non-quadratic manner, namely $\propto n_l^{3/2}$, with the occupancy n_l of that well, which implies that the effective on-site interaction parameters U_l appearing in the Bose–Hubbard Hamiltonian (A.1) scale as $n_l^{-1/2}$ with the occupancies of the corresponding sites. For weakly populated lattice sites that are located at the edge of the atomic cloud, on the other hand, we can justify the perturbative approximation $g \simeq 2\hbar\omega_\perp a_s$ [40] for the effective 1D interaction strength with $a_s \simeq 5.3 \times 10^{-9}$ m the s -wave scattering length of ^{87}Rb atoms, which yields $U_l \simeq 2\hbar\omega_\perp a_s / (\sqrt{2\pi} a_0)$ for those sites.

In order to simultaneously account for weakly and strongly occupied sites of the lattice, we employ a heuristic interpolation formula

$$U_l = \frac{2\hbar\omega_\perp a_s / (\sqrt{2\pi} a_0)}{\sqrt{1 + 4n_l a_s / (\sqrt{2\pi} a_0)}} \quad (\text{A.9})$$

between the perturbative and the Thomas–Fermi regime [41]. We furthermore make the simplifying assumption that the lattice site occupancies n_l remain fairly constant and are not substantially altered in the course of time evolution. While this constraint appears to be well respected on average, significant fluctuations of the lattice site occupancies about their average values may nevertheless arise if the condensate undergoes a transition to a staggered state (as seen in figure 2(b)).

Having thereby determined all relevant parameters of the Bose–Hubbard system (A.1), we can then derive the discrete nonlinear Schrödinger equation

$$\begin{aligned} i\hbar \frac{d}{dt} \psi_l(t) &= -J [\psi_{l+1}(t) e^{i\theta(t)} + \psi_{l-1}(t) e^{-i\theta(t)}] \\ &\quad + V_l \psi_l(t) + U_l [|\psi_l(t)|^2 - 1] \psi_l(t) \end{aligned} \quad (\text{A.10})$$

by means of which the classical fields ψ_l that sample the quantum many-body state of the system have to be evolved with time in the framework of the TW method. For the initial state we assume the presence of a perfect BEC within the optical lattice, which is in an idealized manner described by a coherent state in the classical field space. This leads to the choice $\psi_l(0) = \phi_l + \chi_l$ for the initial value of ψ_l where ϕ_l corresponds to the condensate wavefunction within the (unshaken) lattice at $t = 0$. In practice, ϕ_l is determined by imaginary-time propagation of the Gross–Pitaevskii equation that describes the condensate at $t = 0$ (which is nearly identical with

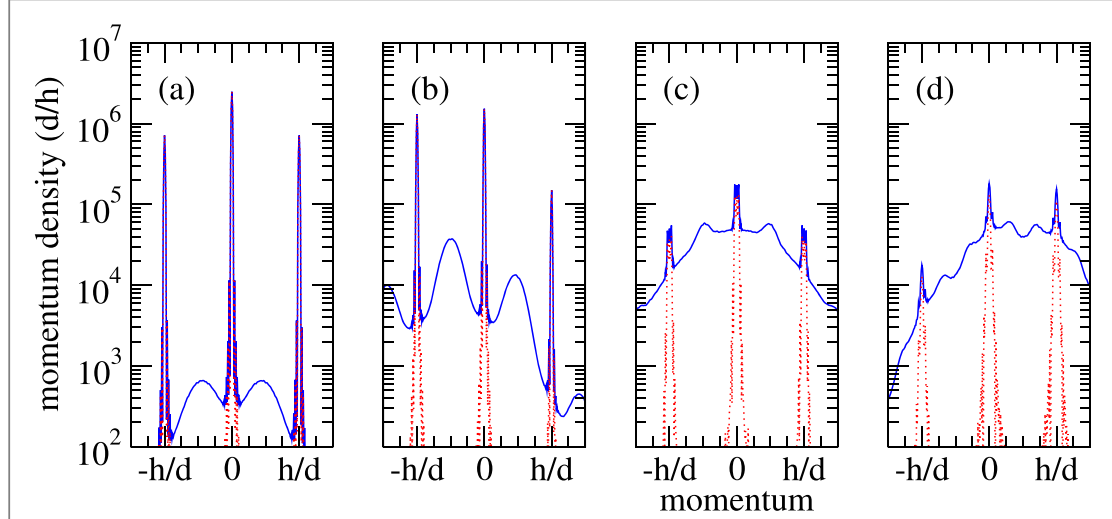


Figure A1. Numerically computed density of atoms in momentum space calculated for the driving frequency $\nu = 1.5$ kHz and the amplitude $\varphi_0 = 0.75\pi$ at the evolution times (a) $t = 2.5$ ms, (b) $t = 5$ ms, (c) $t = 7.5$ ms, and (d) $t = 10$ ms. The lattice depth is $V_0 = 2.6E_L$. The blue solid line represents the total mean density in momentum space computed with the truncated Wigner method, while the red dashed line shows the coherent part of the density which is calculated according to the prescription indicated in equation (A.12).

equation (A.10), except that it exhibits real hopping and the usual $U|\psi_l|^2\psi_l$ interaction term). This thereby yields $n_l = |\phi_l|^2$ for the determination of the on-site interaction strengths according to equation (A.9). χ_l is a complex random number drawn from a Gaussian probability distribution which is centered about the origin in the complex plane and yields the variance $|\chi_l|^2 = 1/2$. Effects due to the presence of finite temperature and initial quantum depletion within the atomic cloud are therefore neglected in this study.

Expectation values of one-body operators are then evaluated according to the prescription

$$\langle \hat{b}_l^\dagger \hat{b}_l + \hat{b}_{l'}^\dagger \hat{b}_l \rangle_t = 2\overline{\psi_l^*(t)\psi_{l'}(t)}, \quad (\text{A.11})$$

where $\overline{\psi_l^*(t)\psi_{l'}(t)}$ denotes the statistical average (over TW trajectories) of the expression $\psi_l^*(t)\psi_{l'}(t)$. This yields in particular $\langle \hat{b}_l^\dagger \hat{b}_l \rangle_t = \overline{|\psi_l(t)|^2} - 1/2$ for the average occupancy of the site l at time t . A similar subtraction of a ‘half-particle’ is needed in order to determine the average distribution of atoms in momentum space.

The TW method also allows one to estimate the remaining condensate fraction within the atomic cloud, namely through the coherent part of one-body observables $\hat{b}_l^\dagger \hat{b}_{l'}$ defined by

$$\langle \hat{b}_l^\dagger \hat{b}_{l'} \rangle_t^{\text{coh}} = \overline{\psi_l^*(t)} \overline{\psi_{l'}(t)}. \quad (\text{A.12})$$

The non-condensed fraction associated with the population of the site l is then approximately determined as

$$\langle \hat{b}_l^\dagger \hat{b}_l \rangle_t - \langle \hat{b}_l^\dagger \hat{b}_l \rangle_t^{\text{coh}} = \overline{|\psi_l(t)|^2} - |\overline{\psi_l(t)}|^2 - 1/2. \quad (\text{A.13})$$

Performing a similar calculation in momentum space, we thereby find in our numerical simulations that many-body coherence is entirely lost in the two side peaks associated with the staggered populations S_\pm shown in figure 2, while it is still preserved within the central peak at $p = 0$ as well as within the side peaks at $p = \pm h/d$. This is shown in figure A1.

Appendix B. Bright solitons in periodically driven Bose–Hubbard systems

In this section, we outline the theory of bright solitons within repulsively interacting BEC that are prepared in periodically driven 1D optical lattices. Our starting point is the simplified Bose–Hubbard Hamiltonian (4) which assumes the presence of a homogeneous optical lattice of infinite extension. A BEC prepared within this lattice therefore evolves according to the discrete nonlinear Schrödinger equation

$$i\hbar \frac{\partial}{\partial t} \psi_l(t) = -\bar{J}[\psi_{l+1}(t) + \psi_{l-1}(t)] + U|\psi_l(t)|^2\psi_l(t), \quad (\text{B.1})$$

where $U > 0$ represents the on-site interaction strength and \bar{J} is the effective renormalized tunneling rate according to equation (3).

For $\bar{J} < 0$, equation (B.1) admits approximate solitonic solutions of the form

$$\psi_l(t) = \sqrt{n_0} \operatorname{sech}[(l - l_0)/w] e^{-i\mu t/\hbar}, \quad (\text{B.2})$$

which correspond to a hyperbolic secant function $\operatorname{sech}(x) \equiv 1/\cosh(x)$ centered about some lattice site index $l_0 \in \mathbb{Z}$ with the peak density n_0 and the characteristic width w in terms of the lattice spacing. Indeed, we can approximately express

$$\psi_{l+1}(t) + \psi_{l-1}(t) \simeq 2\psi_l(t) + \frac{\partial^2}{\partial l^2}\psi_l(t) \quad (\text{B.3})$$

for $w \gg 1$ and evaluate

$$\frac{\partial^2}{\partial l^2}\psi_l(t) = \frac{1}{w^2}\psi_l(t) - \frac{2}{n_0 w^2}|\psi_l(t)|^2\psi_l(t) \quad (\text{B.4})$$

using $\operatorname{sech}''(x) = \operatorname{sech}(x) - 2\operatorname{sech}^3(x)$ for all $x \in \mathbb{R}$. Inserting the expressions (B.3) and (B.4) into the discrete Gross–Pitaevskii equation (B.1) yields the relation

$$w = \sqrt{\frac{-2\bar{J}}{U n_0}} \quad (\text{B.5})$$

between the width w and the height n_0 of the soliton. Its associated chemical potential

$$\mu = -2\bar{J} + \frac{1}{2}U n_0 \quad (\text{B.6})$$

is located within the band gap above the ground band of the driven optical lattice.

From the shape of the hyperbolic secant function we infer the FWHM of the gap soliton as

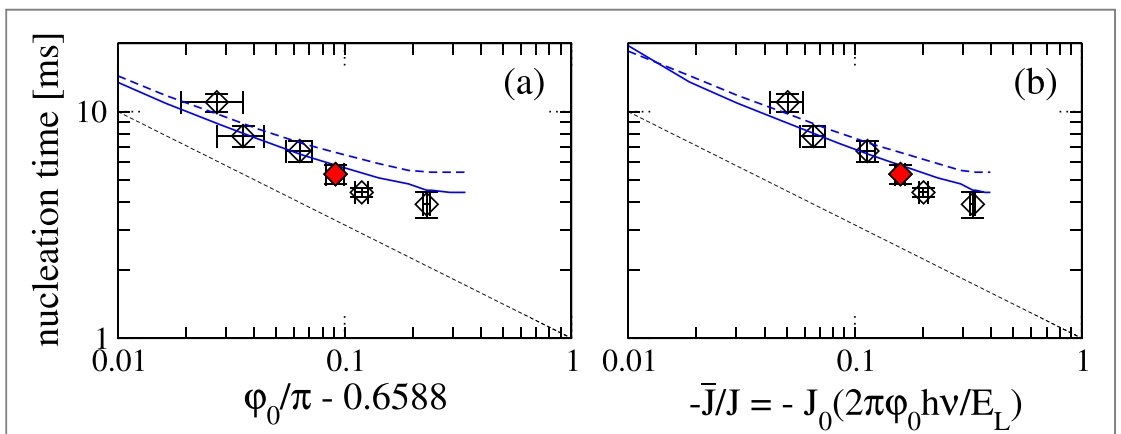
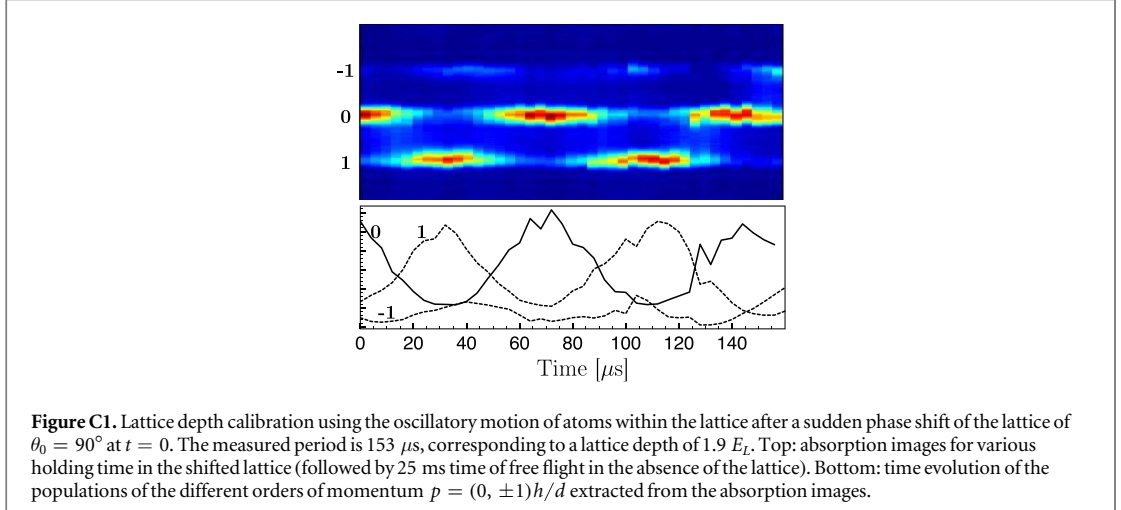
$$\sigma \simeq 2.634 wd = 2.634 \sqrt{\frac{-2\bar{J}}{U n_0}} d, \quad (\text{B.7})$$

where d is the lattice period. For the experiment shown in figure 1(a), which was done with the shaking amplitude $\varphi_0 = 0.75\pi$ yielding $\bar{J} \simeq -0.16J$ and which featured an average occupancy of some 3300 atoms per lattice site as can be seen in figure 2(b), we obtain through equations (A.6) and (A.9) $\bar{J}/U \simeq 180$ on average within the lattice. Inferring again from figure 2(b) a peak height of the order of $n_0 \simeq 5000$, we finally obtain $\sigma \simeq 0.7 d$ for the FWHM width of the soliton, which is in fairly good agreement with the TW calculation shown in figure 2(b).

We should note that the above reasoning is rather approximate insofar as we cannot *a posteriori* justify the approximation (B.3) for such narrow widths. This is reflected by the fact that the spiky peaks shown in figure 2(b) are not really isolated from each other in a solitary manner, but rather form a dense array. Their occurrence gives rise to an enhancement of the total interaction energy contained within the atomic gas (as would any inhomogeneity in the spatial density distribution), and this enhancement compensates for the loss of kinetic energy that is associated with the transfer of atoms from the condensate state in the presence of the driving at $k = 0$ (highly energetic) to the staggered state characterized by $k = \pm\pi/d$ (lowly energetic). This situation is perfectly complementary to the formation of conventional bright solitons within an attractively interacting 1D BEC, where the enhancement of kinetic energy due to the loss of homogeneity would be compensated by the gain of interaction energy.

Appendix C. Lattice depth calibration

We perform a precise calibration of the lattice depth using the out-of-equilibrium dynamics of a chain of BECs in an optical lattice following the method we demonstrated in [26]. To do so, we first load adiabatically a BEC in the lattice, creating a chain of BECs trapped at the bottom of the lattice sites. At $t = 0$, we suddenly shift the phase of the lattice, which triggers the center-of-mass motion of the atomic wave packets in each well (shift of $\theta_0 = 90^\circ$ here). After a given holding time in the shifted lattice, we perform a 25 ms time-of-flight. The experimental absorption images (see figure C1) show the interferences of the different wave packets located in each lattice site. The interference figure is centered on the central interference peak (0th order) corresponding to wave packets that were released while being at rest in the shifted lattice, i.e. at the turning points of the oscillatory motion. We observe oscillations of the population in the 0th order from which we extract the period of the center-of-mass motion of the atomic wave packets. This period can be directly related to the depth of the optical lattice. Indeed, the intrasite dipole mode is coupled to a two phonon transition between the ground state band and the second excited band at $k = 0$:



$$T_c = \frac{1}{\nu_c} = \frac{2h}{E_3(k=0) - E_1(k=0)}. \quad (\text{C.1})$$

In this way, we find a lattice of depth $1.9 E_L$ corresponding to the measured period $T_c = 153 \mu\text{s}$. Interestingly, we have shown that this kind of measurement is robust against the value of the phase shift of excitation θ_0 , the atom–atom interaction strength, and the external confinement superimposed to the lattice. For these values of the phase shift and the lattice depth, tunneling plays an important role in the wave packet dynamics insofar as an important fraction of the wave packets tunnels to the neighboring lattice sites. It explains for instance the population of the -1 order for an evolution time in the shifted lattice of $40 \mu\text{s}$ but also more generally the asymmetry of the populations in the ± 1 orders. We have studied in details such effect in [26].

Appendix D. Parameter ranges for the nucleation of staggered states

This section is devoted to a more extensive discussion of the parameter ranges within which a nucleation of staggered states can be observed. We start by recalling that the dependence of the nucleation time with the driving amplitude φ_0 is studied in detail within figure 1. As key feature we find that the nucleation time diverges when φ_0 approaches the value 0.6588π where the Bessel function appearing within equation (3) of the main text has its first node. Identifying this nucleation time approximately with the inverse of the Lyapunov exponent $\lambda = [-8\bar{J}(2\bar{J} + nU)]^{1/2}/\hbar$ that characterizes the dynamical instability of the condensate, and assuming an approximately linear scaling (with negative slope) of the effective renormalized tunneling rate \bar{J} with the distance of φ_0 from the node of the Bessel function, we should expect that the nucleation time diverges as

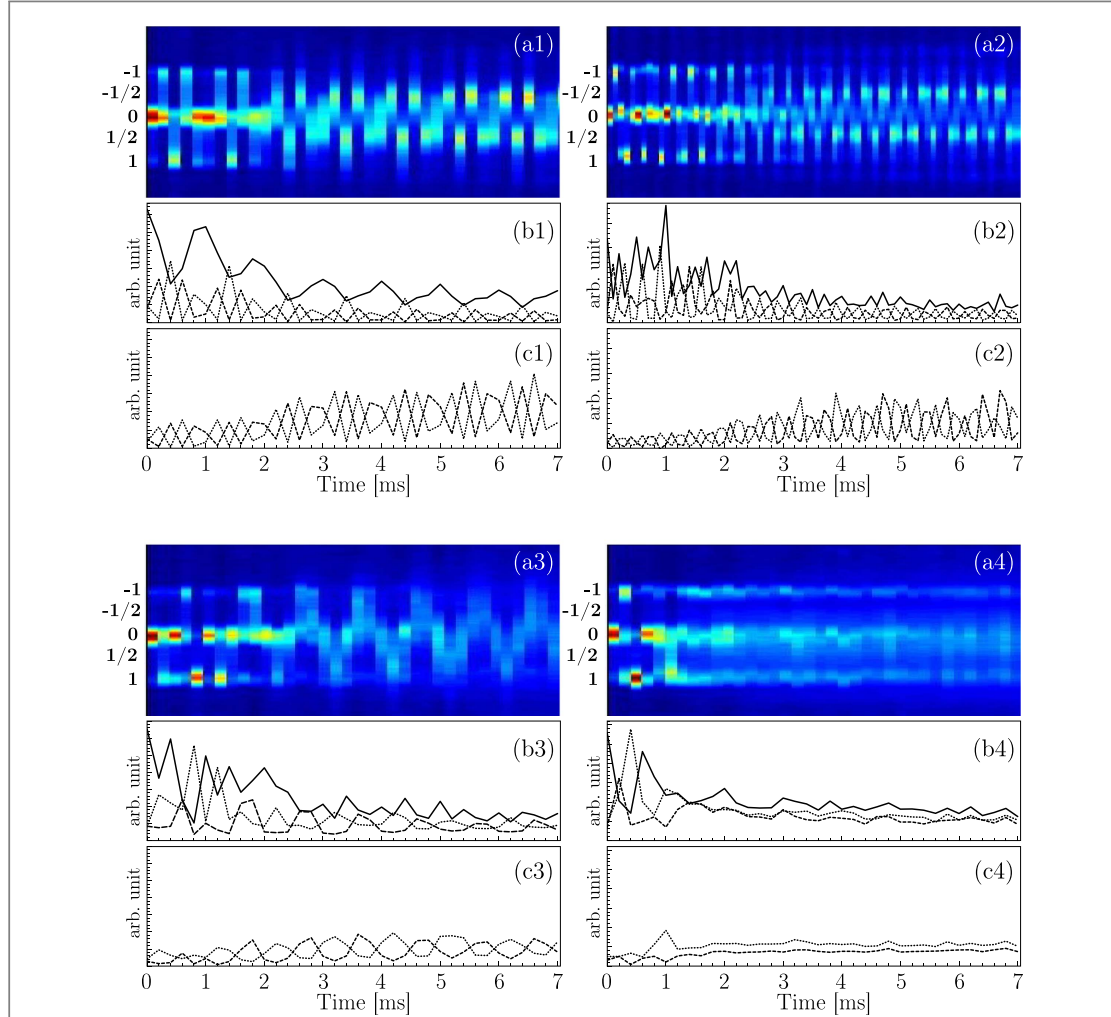


Figure D2. Nucleation of the staggered states for different modulation frequency ν . For (1–4), the modulation frequencies are below the center-of-mass oscillation frequency ($\nu_c = 6.55$ kHz, corresponding to a lattice depth of $1.9 E_L$). The product $\varphi_0\nu$ with φ_0 the amplitude of modulation is kept constant, corresponding to a negative renormalized tunneling rate \bar{J} . The (amplitude,frequency) couple takes the following values (1) $(0.67\pi, 2$ kHz), (2) $(0.44\pi, 3$ kHz), (3) $(0.33\pi, 4$ kHz) and (4) $(0.27\pi, 5$ kHz). For every set of values are represented: (a) absorption images obtained for various evolution times followed by 25 ms time-of-flight, where the time step is set to 100 μ s for the measurement (2) and 200 μ s for the other measurements; (b), (c) time evolution of the population in the different orders of momentum $p = (0, \pm 1/2, \pm 1) h/d$ extracted from the absorption images, with the orders (b) 0 (solid), +1 (dashed), -1 (dotted) and (c) +1/2 (dashed), -1/2 (dotted).

$\sim(\varphi_0 - 0.6588\pi)^{-1/2}$ when approaching the node of the Bessel function. As we can see in figure D1, this is indeed confirmed when plotting the experimental and numerical nucleation time data of figure 1(b) in a double logarithmic representation.

D.1. Frequency range

We extend the study of the effect of the modulation frequency ν on the nucleation of staggered states performed in the main article to determine the frequency range in which such states appear. We first use a lattice of depth $1.9 E_L$, characterized by a center-of-mass oscillation of frequency $\nu_c = 6.55$ kHz (see above) and perform phase modulation experiments at different modulation frequencies below ν_c (see figure D2 (1–4)). We maintain the product $\varphi_0\nu$ constant with φ_0 the amplitude of modulation, yielding an effective tunneling rate \bar{J} that is constant and negative. The argument of the Bessel function (see equation (3)) is chosen equal to 3.24.

At the lowest modulation frequencies (2 and 3 kHz), we clearly observe the nucleation of staggered states with the population of staggered modes at momentum $p = \pm h/2d$, whereas for larger modulation frequencies ($\nu = 5$ kHz), we do not significantly populate the staggered modes (see figure D2(c4)). More specifically, we observe the population of staggered modes for modulation frequencies up to typically $\nu_c/2$, meaning for modulation frequencies that are not too close to excitations frequencies towards the excited bands. The experiments presented in figure 3 on the effect of the modulation frequency were performed with a lattice of depth $2.6 E_L$, corresponding to a center-of-mass oscillation frequency $\nu_c = 8.1$ kHz. As those experiments were

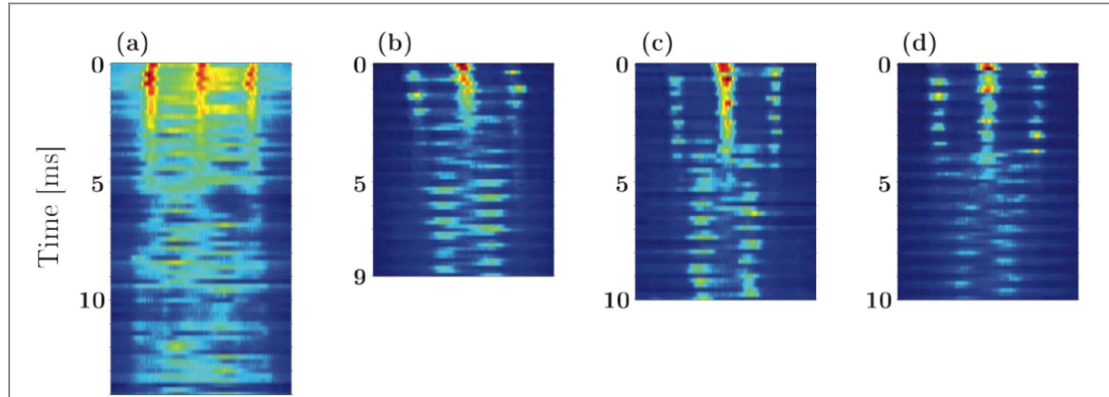


Figure D3. Nucleation of the staggered states for different lattice depths: (a) $1.2 E_L$, (b) $1.8 E_L$, (c) $2.6 E_L$ and (d) $3.2 E_L$. The absorption images are obtained for various evolution times followed by 25 ms time-of-flight. The amplitude φ_0 and frequency ν of modulation have been chosen such to keep the argument of the Bessel function (see equation (3)) equal to 3.24: (a) $\varphi_0 = 1.67\pi$ and $\nu = 800$ Hz (b)–(d) $\varphi_0 = 0.89\pi$ and $\nu = 1.5$ kHz.

performed for modulation frequencies up to 4 kHz, we could see the population of the staggered modes for each chosen modulation frequency.

D.2. Lattice depth range

We perform phase modulation experiments for different lattice depths ranging from $1.2 E_L$ to $3.2 E_L$ and observe the nucleation of staggered states in this range of lattice depth (see figure D3). The product $\varphi_0 \times \nu$ is kept constant and corresponds to a negative effective tunneling rate \bar{J} . The dynamics for the population of staggered modes look similar to the dynamics shown in figure 1, but for the lattice depth $1.2 E_L$. For the lattice depth $1.2 E_L$, the measurement is performed at a lower modulation frequency and as a consequence with a larger amplitude of modulation. For such an amplitude of modulation, the associated classical phase space starts to exhibit chaotic zones, which is probably responsible for the disrupted aspect of the dynamics observed in this case (see figure D3(a)).

References

- [1] Dalfovo F, Giorgini S, Pitaevskii L P and Stringari S 1999 *Rev. Mod. Phys.* **71** 463
- [2] Giorgini S, Pitaevskii L P and Stringari S 2008 *Rev. Mod. Phys.* **80** 1215
- [3] Bloch I, Dalibard J and Zwerger W 2008 *Rev. Mod. Phys.* **80** 885
- [4] Bloch I, Dalibard J and Nascimbène S 2012 *Nat. Phys.* **8** 267
- [5] Gemelke N, Sarajlic E, Bidel Y, Hong S and Chu S 2005 *Phys. Rev. Lett.* **95** 170404
- [6] Lignier H, Sias C, Ciampini D, Singh Y, Zenesini A, Morsch O and Arimondo E 2007 *Phys. Rev. Lett.* **99** 220403
- [7] Kierig E, Schnorrberger U, Schietinger A, Tomkovic J and Oberthaler M K 2008 *Phys. Rev. Lett.* **100** 190405
- [8] Goldman N and Dalibard J 2014 *Phys. Rev. X* **4** 031027
- [9] Hofstetter D R 1976 *Phys. Rev. B* **14** 2239
- Aidelsburger M, Atala M, Nascimbène S, Trotzky S, Chen Y-A and Bloch I 2011 *Phys. Rev. Lett.* **107** 255301
- Aidelsburger M, Atala M, Lohse M, Barreiro J T, Paredes B and Bloch I 2013 *Phys. Rev. Lett.* **111** 185301
- Miyake H, Siviloglou G A, Kennedy C J, Burton W C and Ketterle W 2013 *Phys. Rev. Lett.* **111** 185302
- Aidelsburger M, Lohse M, Schweizer C, Atala M, Barreiro J T, Nascimbène S, Cooper N R, Bloch I and Goldman N 2015 *Nat. Phys.* **11** 162
- Haldane F D M 1988 *Phys. Rev. Lett.* **61** 2015
- Jotzu G, Messer M, Desbuquois R, Lebrat M, Uehlinger T, Greif D and Esslinger T 2014 *Nature* **515** 237
- Struck J, Ölschläger C, Le Targat R, Soltan-Panahi P, Eckardt A, Lewenstein M, Windpassinger P and Sengstock K 2011 *Science* **333** 996
- Struck J et al 2013 *Nat. Phys.* **9** 738
- Parker C V, Ha L-C and Chin C 2013 *Nat. Phys.* **9** 769
- Clark L W, Feng L and Chin C 2016 *Science* **354** 606
- Feng L, Clark L W, Gaj A and Chin C 2018 *Nat. Phys.* **14** 269
- Weinberg M, Ölschläger C, Sträter C, Prelle S, Eckardt A, Sengstock K and Simonet J 2015 *Phys. Rev. A* **92** 043621
- Reitter M, Nägerl J, Wintersperger K, Sträter C, Bloch I, Eckardt A and Schneider U 2017 *Phys. Rev. Lett.* **119** 200402
- Görg F, Messer M, Sandholzer K, Jotzu G, Desbuquois R and Esslinger T 2018 *Nature* **553** 481–5
- Glauber R J 1963 *Phys. Rev.* **130** 2529
- Hilligsøe K M and Mølmer K 2005 *Phys. Rev. A* **71** 041602
- Campbell K K, Mun J, Boyd M, Streed E W, Ketterle W and Pritchard D E 2006 *Phys. Rev. Lett.* **96** 020406
- Lellouch S, Bukov M, Demler E and Goldman N 2017 *Phys. Rev. X* **7** 021015
- Pedri P, Pitaevskii L, Stringari S, Fort C, Burger S, Cataliotti F S, Maddaloni P, Minardi F and Inguscio M 2001 *Phys. Rev. Lett.* **87** 220401
- Madison K W, Chevy F, Wohlleben W and Dalibard J 2000 *Phys. Rev. Lett.* **84** 806
- Smith N L, Heathcote W H, Krueger J M and Foot C J 2004 *Phys. Rev. Lett.* **93** 080406

- [23] Haljan P C, Coddington I, Engels P and Cornell E A 2001 *Phys. Rev. Lett.* **87** 210403
- [24] Sinha S and Castin Y 2001 *Phys. Rev. Lett.* **87** 190402
- [25] Lobo C, Sinatra A and Castin Y 2004 *Phys. Rev. Lett.* **92** 020403
- [26] Fortun A, Cabrera-Gutiérrez C, Condon G, Michon E, Billy J and Guéry-Odelin D 2016 *Phys. Rev. Lett.* **117** 010401
- [27] Dunlap D H and Kenkre V M 1986 *Phys. Rev. B* **34** 3625
- [28] Eckardt A, Weiss C and Holthaus M 2005 *Phys. Rev. Lett.* **95** 260404
- [29] Eckardt A 2017 *Rev. Mod. Phys.* **89** 011004
- [30] Castin Y and Dum R 1998 *Phys. Rev. A* **57** 3008
- [31] Steel M J, Olsen M K, Plimak L I, Drummond P D, Tan S M, Collett M J, Walls D F and Graham R 1998 *Phys. Rev. A* **58** 4824
Sinatra A, Lobo C and Castin Y 2002 *J. Phys. B: At. Mol. Opt. Phys.* **35** 3599
Gardiner C and Zoller P 2004 *Quantum Noise* 3rd edn (Berlin: Springer)
Polkovnikov A 2010 *Ann. Phys.* **325** 1790
- [32] Dujardin J, Engl T, Urbina J D and Schlagheck P 2015 *Ann. Phys.* **527** 629
- [33] Sträter C and Eckardt A 2016 *Z. Naturforsch.* **71** 909
- [34] Abanin D A, De Roeck W, Ho W W and Huveneers F 2017 *Phys. Rev. B* **95** 014112
- [35] Hadzibabic Z, Krüger P, Cheneau M, Battelier B and Dalibard J 2006 *Nature* **441** 1118
- [36] Eiermann B, Anker Th, Albiz M, Taglieber M, Treutlein P, Marzlin K-P and Oberthaler M K 2004 *Phys. Rev. Lett.* **92** 230401
- [37] Mamaev A V, Saffman M and Zozulya A A 1995 *Phys. Rev. Lett.* **76** 2262
Anderson B P, Haljan P C, Regal C A, Feder D L, Collins L A, Clark C W and Cornell E A 2001 *Phys. Rev. Lett.* **86** 2926
- [38] Reinaudi G, Lahaye T, Wang Z and Guéry-Odelin D 2007 *Opt. Lett.* **32** 3143
- [39] Landau LD and Lifshitz I M 1965 *Quantum Mechanics* (Oxford: Pergamon)
- [40] Garg A 2000 *Am. J. Phys.* **68** 430
- [41] Olshanii M 1998 *Phys. Rev. Lett.* **81** 938
- [42] Paul T, Hartung M, Richter K and Schlagheck P 2007 *Phys. Rev. A* **76** 063605